Electronic Supplementary Information

Synergistic Spin-State Modulation in Co/N co-Doped TiO_2 for Enhanced Photoelectrocatalytic Oxygen Evolution under External Magnetic Fields

Dibyendu Ghosh[1,2], Krishnendu Roy[1], Soumyajit Maitra[1], and Praveen Kumar[1,3,*]

[1]*School of Materials Science, Indian Association for the Cultivation of Science, Kolkata 700032, India.*

[2]*Department of Physics, Sister Nivedita University, DG 1/2 New Town, Action Area 1, Kolkata 700156*

[3]*Plaksha University, Sahibzada Ajit Singh Nagar, Mohali-140306, India*

**Corresponding Author Email: praveen.kumar@plaksha.edu.in*

MATERIALS AND METHODS

Materials: Titanium isopropoxide ((Merck), Thiourea (99%, Sigma-Aldrich)), Cobalt acetate tetrahydrate (99%, Sigma-Aldrich), 2-Propanol (Merck), Acetone (Merck), Hydrazine hydrate (80%, Sigma-Aldrich), Sulfuric acid (98%, Merck).

Synthesis Protocol:

TiO_2 nanoparticle: In a typical synthesis procedure of TiO_2 nanoparticles was prepared using typical sol-gel method.[1] 1 ml (0.17 mol) Titanium isopropoxide was slowly dropwise added to a beaker containing 20 ml of Ethanol and water (3:1) under vigorous stirring. The stirring was done for 2 h then the white precipitate was centrifuged and washed 2-3 times. The TiO_2 nanoparticles was then dry overnight under vacuum and heated at 550^{o}C for 1 h.

N-doped and Co/N co-doped TiO_2: The N-doped and Co/N co-doped TiO_2 synthesis combined the sol-gel and precipitation methods along with the N precursor as thiourea (0.5 mol for NTO-1 to 1.5mol for NTO-4) and Co precursor cobalt acetate tetrahydrate (0.05 mol-0.15 mol) previously dissolved in the 20 ml of Ethanol and water (3:1). Following the same washing and heating process as TiO_2, NTO and CoNTO samples were prepared by varying the thiourea 0.1-0.3 M and cobalt acetate tetrahydrate 0.05-1.5 M.

Computational Details: DFT calculations have been carried out using the CASTEP code. Band structure and DOS plots were carried out using a 9x9x3 Monkhorst pack scheme k point grid using GGA exchange-correlation with PBE functional using Norm Conserving Pseudopotentials, Koelling-Hammon relativistic treatment with plane-wave basis set cutoff set to 1350 eV and SCF cutoff set at $1e^{-7}$ eV.[2-5] Spin-orbit coupling was included in the calculations. Pulay Density mixing scheme was used as an electronic minimizer. PBE+D2 correction using Grimme parameters to take into account vdW interactions were included.[6] According to previous reports,[5] slab models were constructed with a 30 Å vacuum layer to prevent interlayer interaction with a 5x5x1 k point grid and all other parameters remaining the same. Geometry optimization was carried out using the BFGS algorithm with maximum energy cutoff set at $1e^{-7}$ eV, maximum force, maximum stress, and maximum displacement set at 0.01 eV/Å, 0.03 Gpa, and 0.001 Å, respectively. Spin orbital coupling was included in geometry optimization as well. According to previous reports, a Brillouin Zone path of Γ→M→K→Γ→K' was used.[7]

PEC characterization: The final PEC devices were characterize using an electrochemical workstation (Bio-Logic Science Instruments, Model SP-300) in a typical three-electrode configuration with Pt as counter electrode and saturated calomel electrode (SCE) as a reference in the 1M NAOH electrolyte, and the illumination source was a 100 W AM 1.5G solar simulator (PECCEL, Japan, Model: L-01). The three electrodes PEC device and EIS measurements were performed in three-neck glass cells with FTO/TiO_{2-x}, FTO/NTO and FTO/CoNTO as a working electrode, Pt as a counter electrode, and Hg/HgO electrode as a reference electrode. 1 M NAOH electrolyte was used for all PEC characterization. The quantities of evolved gases were measured by Gas chromatography (GC) analysis by an online GC analyzer (Model. TRACE 1300, Thermo Fisher)

Material Characterization. Morphological characterization *via* FESEM micrograph was recorded by JEOL JSM 7500F. Elemental analysis via EDX was recorded using Oxford Instruments X-Max with INCA software coupled to the FESEM. TEM and HAADF-STEM images with elemental mapping were recorded with JEOL, JEM-2100F coupled with EDX setup, and 200 kV electron source. The XRD measurements were carried out with a Rigaku (Mini Flex II, Japan) powder X-ray diffractometer having Cu Kα = 1.54059 Å radiation. Raman spectra were recorded using Horiba T64000 Raman spectrometer with 532 nm laser excitation at 2 mW/cm^2 intensity. XPS spectra were recorded using an Omicron Nanotechnology XPS with a hemispherical analyser and a multichannel detector. UV-vis-NIR absorption spectra were recorded on a Varian Cary 5000 UV-vis-NIR spectrophotometer (175-3300 nm range). MPMS characterization was carried out using the Quantum Design MPMS XL system. The fluorescence lifetimes were recorded by using a time-correlated single-photon counting spectrofluorometer from HORIBA Jobin Yvon IBH. The fluorescence lifetime was calculated by fitting the decay curves by using a program installed by IBH. Circular Dichroism (CD) measurement was carried out using JASCO J-815 spectropolarimeter. CPL measurement was carried out using JASCO CPL-300 Spectrometer.

Table S1:

Material name	Lattice parameter (a) (Å)	Lattice parameter (b) (Å)	Lattice parameter (c) (Å)	Unit cell volume ($Å^3$)
TiO_{2-x}	3.7886	3.7886	9.5230	136.71
NTO-3	3.7966	3.7966	9.4990	136.92
CoNTO-2	3.7935	3.7935	9.5086	136.83

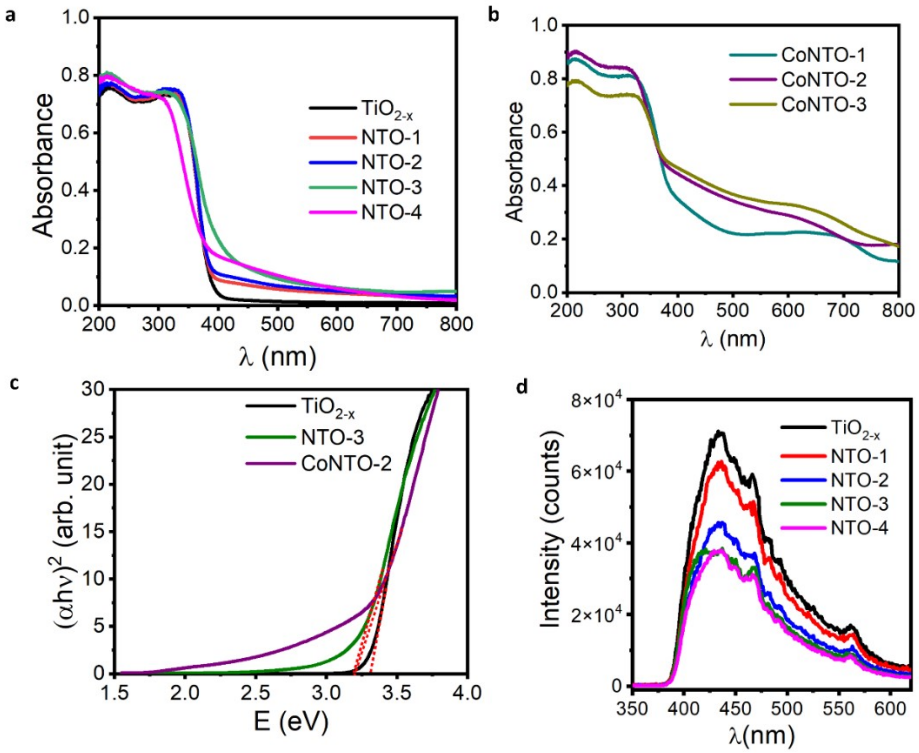

Fig. S1. a) UV-Vis absorption spectra of TiO_{2-x} and various nitrogen-doped TiO_2 (NTO) samples, demonstrating the impact of nitrogen incorporation on optical absorption. b) UV-Vis absorption spectra of CoNTO and various Co doped in NTO-3. c) Tauc plot for TiO_{2-x}, NTO-3 and CoNTO-2. d) Photoluminescence (PL) spectra of different NTO samples, highlighting variations in charge carrier recombination dynamics.

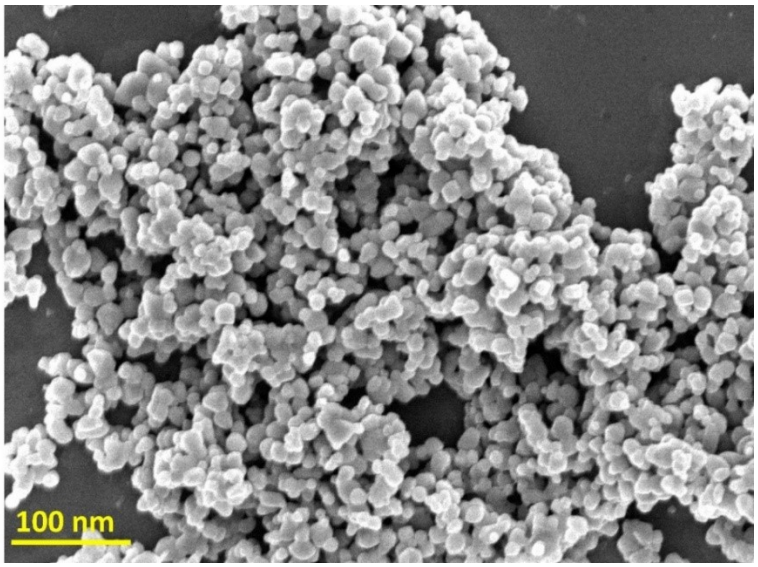

Fig. S2. Scanning electron microscopy (SEM) image of CoNTO-2, illustrating the surface morphology and structural features of the co-doped sample.

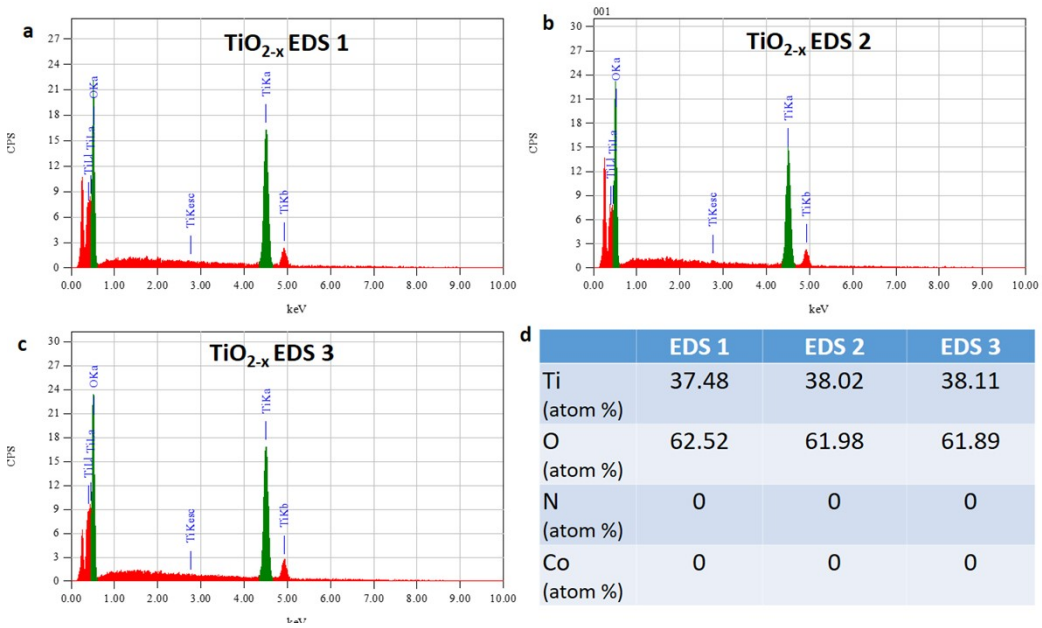

d

	EDS 1	EDS 2	EDS 3
Ti (atom %)	37.48	38.02	38.11
O (atom %)	62.52	61.98	61.89
N (atom %)	0	0	0
Co (atom %)	0	0	0

Fig. S3. a-c) Energy-dispersive X-ray spectroscopy (EDS) spectra of TiO_{2-x} obtained from repeated measurements, confirming elemental composition. d) Elemental analysis data derived from SEM-EDS, providing a quantitative assessment of TiO_{2-x}.

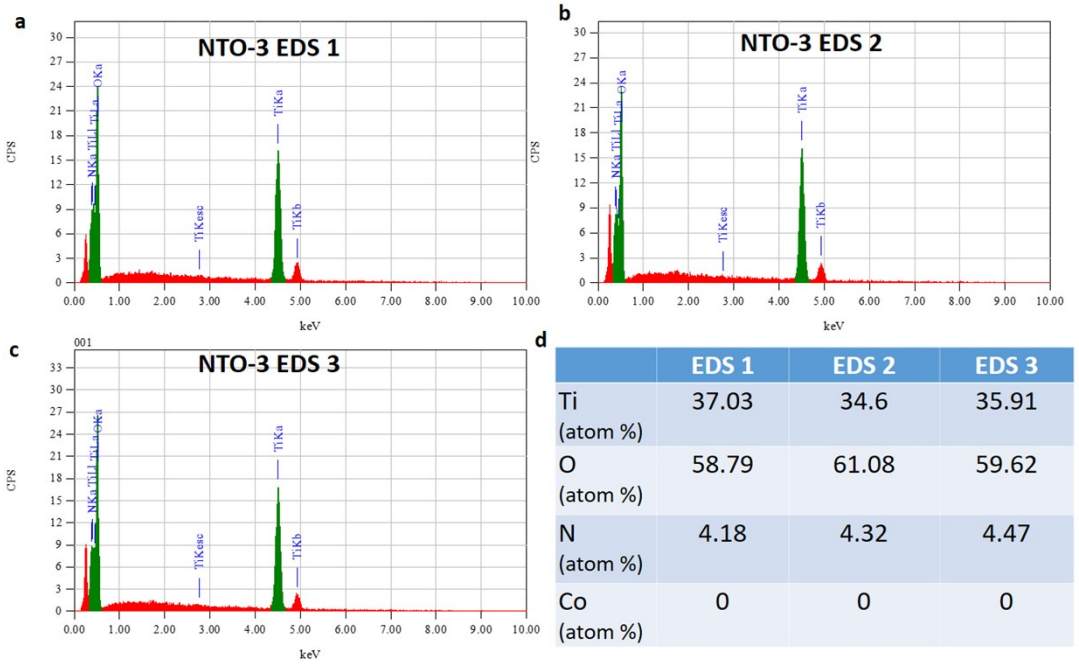

d

	EDS 1	EDS 2	EDS 3
Ti (atom %)	37.03	34.6	35.91
O (atom %)	58.79	61.08	59.62
N (atom %)	4.18	4.32	4.47
Co (atom %)	0	0	0

Fig. S4. a–c) Repeated EDS spectra taken from identical samples of NTO-3, verifying the elemental distribution and doping consistency. d) SEM-EDS-based elemental analysis data of NTO-3, ensuring accurate compositional characterization.

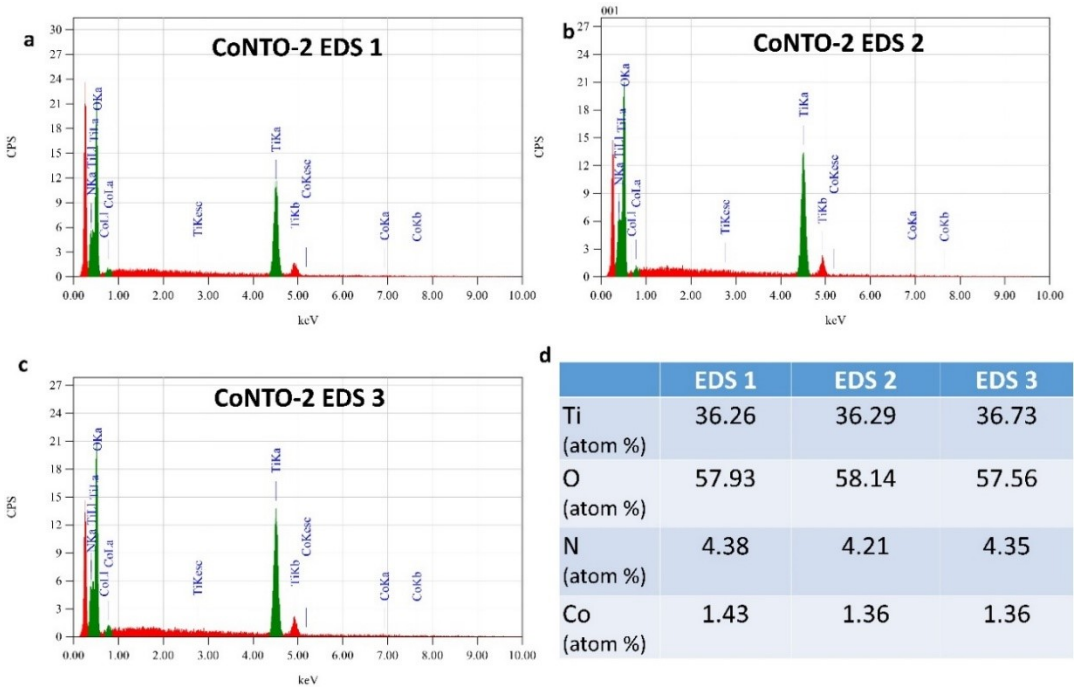

d

	EDS 1	EDS 2	EDS 3
Ti (atom %)	36.26	36.29	36.73
O (atom %)	57.93	58.14	57.56
N (atom %)	4.38	4.21	4.35
Co (atom %)	1.43	1.36	1.36

Fig. S5. a–c) Repeated EDS spectra taken from identical samples of CoNTO-2, validating the uniform incorporation of Co and N into the TiO_2 lattice. d) Elemental analysis data from SEM-EDS, confirming the stoichiometry of CoNTO-2.

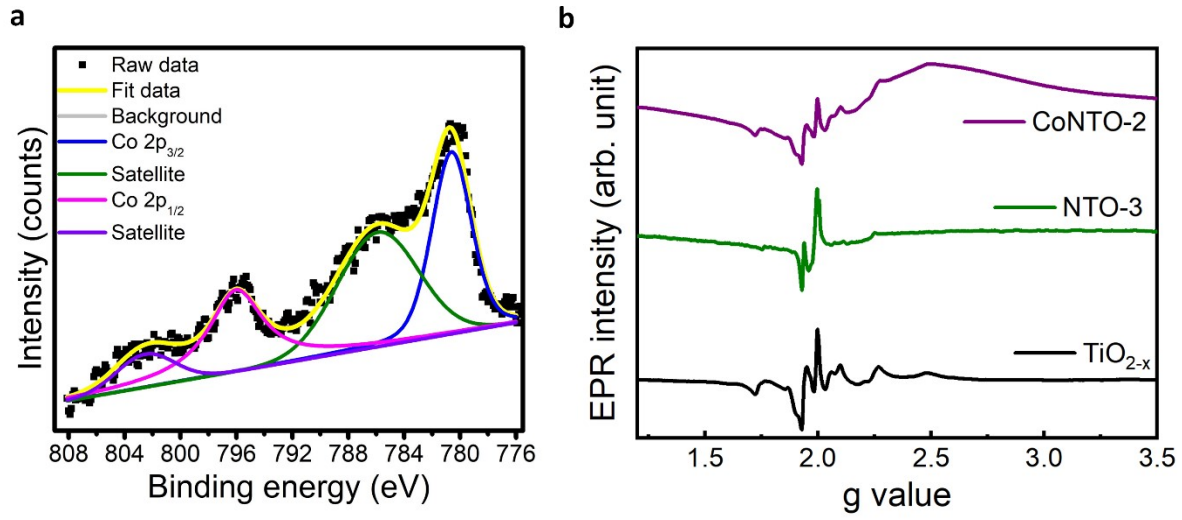

Fig. S6. a) X-ray photoelectron spectroscopy (XPS) spectra of the deconvoluted Co^{2+} peak in CoNTO-2, providing insights into the oxidation state and electronic environment of Co dopants. b) EPR spectra for representative TiO_{2-x}, NTO-3 and CoNTO-2.

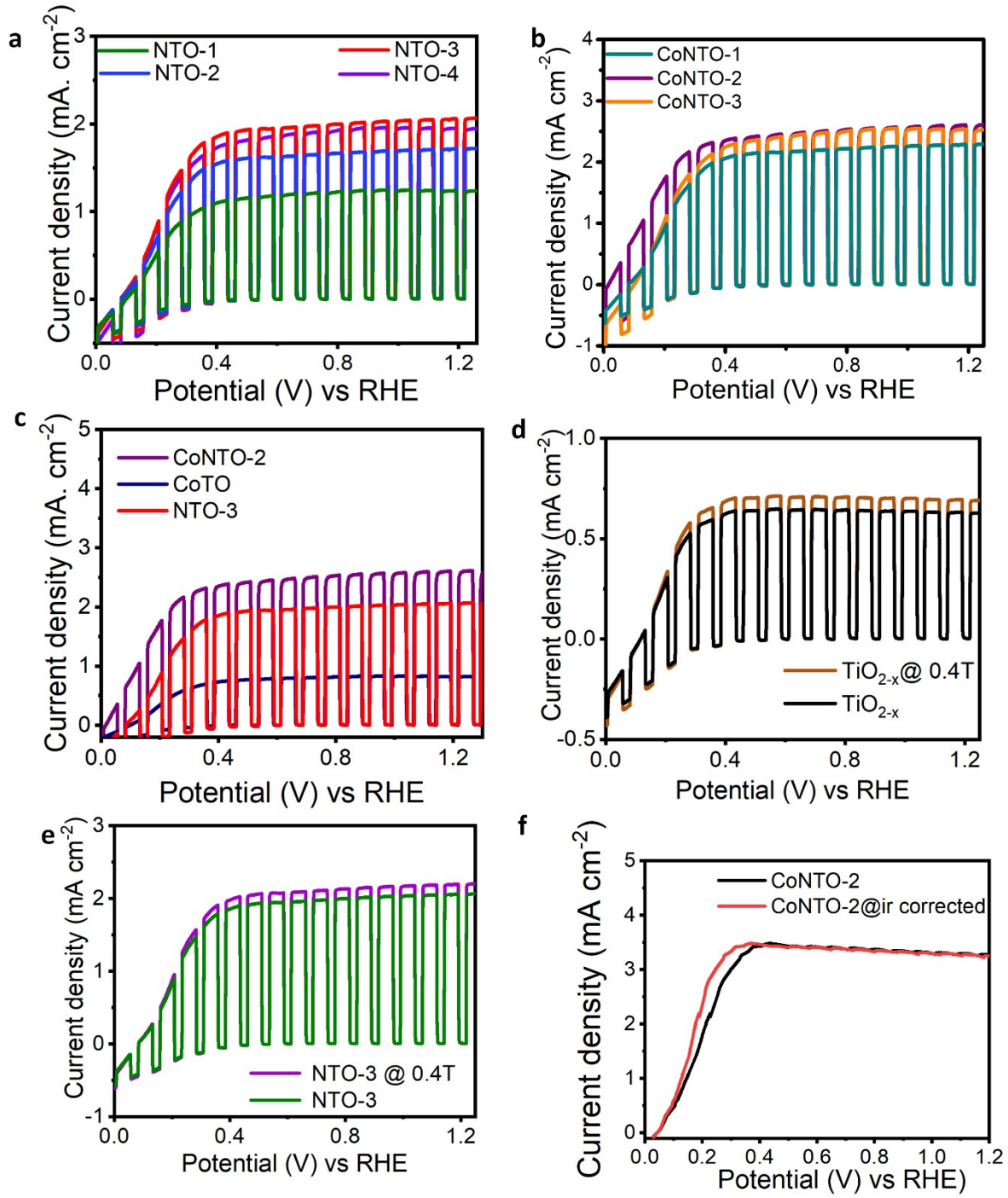

Fig. S7. Chopped LSV for a) NTO and b) CoNTO. c) Chopped LSV for CoTO with NTO-3 and CoTO-2. Chopped LSV under 0.4T magnetic field for d) TiO_{2-x} and a representative e) NTO-3 sample. f) iR corrected LSV for ConTO-2 at 0.4T applied magnetic field.

Supplementary Note 1: The effect of magnetic field of TiO_{2-x} shows slight enhancement in the photocurrent density (Fig. S7c) which signifies the spin polarization in pristine TiO_{2-x}. The representative NTO-3 (Fig. S7d) sample also shows slight enhancement with the magnetic field and this signifies the need of Co doping further.

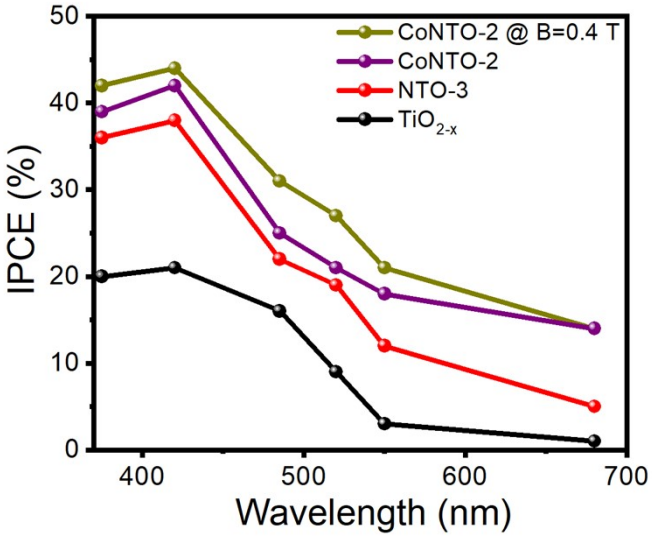

Fig. S8. Incident photon-to-current efficiency (IPCE) spectra of TiO_{2-x}, NTO-3, and CoNTO-2 (H = 0 and 0.4 T), demonstrating enhanced photoresponse due to co-doping and magnetic field effects.

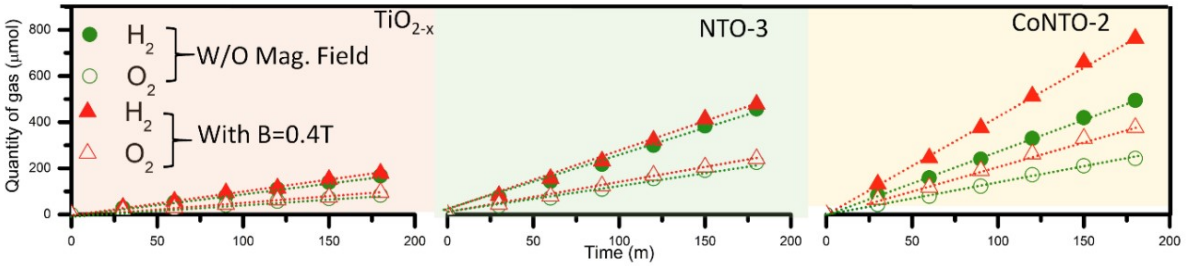

Fig. S9. Gas chromatography (GC) data of three different anode samples, illustrating variations in gas evolution and Faradaic efficiency.

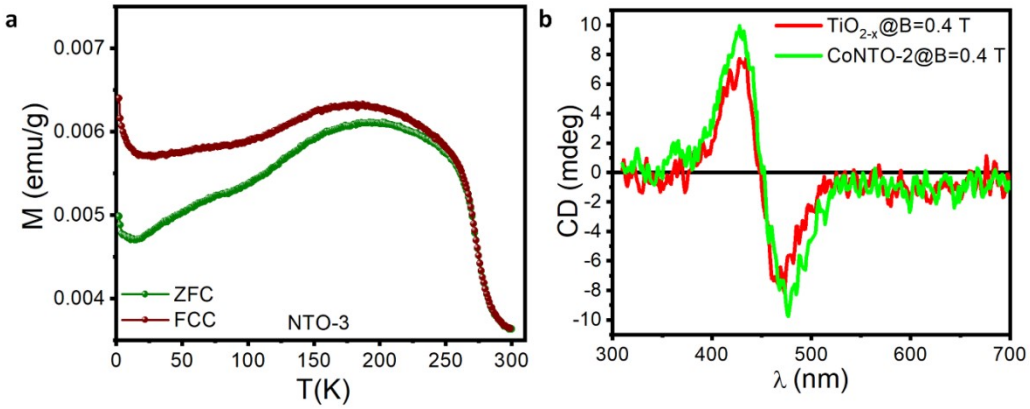

Fig. S10. a) Magnetization vs. temperature (M-T) plot of NTO (3) measured at 500 Oe, assessing the magnetic behavior of nitrogen-doped TiO_{2-x}. b) Circular dichroism (CD) spectra of TiO_{2-x} and CoNTO-2 under an applied magnetic field, providing evidence of magneto-chiral optical activity.

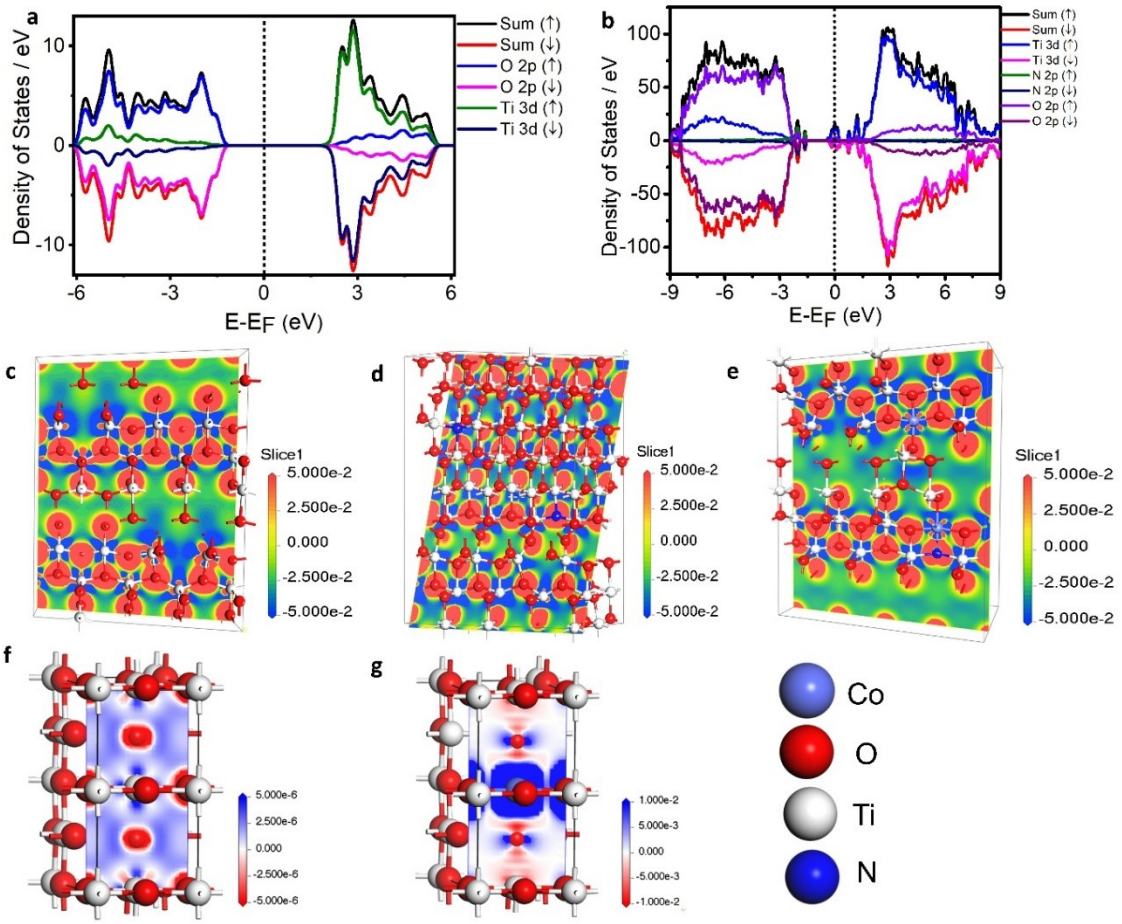

Fig. S11. a) Partial density of states (PDOS) plot of pristine TiO_{2-x}, demonstrating the absence of spin polarization. b) PDOS plot of NTO, revealing minor spin asymmetry due to nitrogen doping. c–e) Hirshfeld charge analysis of c) TiO_{2-x}, d) NTO, and e) CoNTO-2, elucidating charge distribution and electron density at active sites, correlating with catalytic activity. Spin density contour map of (f) TiO_{2-x}, and (g) CoNTO-2

References

1. A. E. Mragui, O. Zegaoui, I. Daou, J. C. G. Esteves da Silva, Synthesis of Fe- and Co-Doped TiO_2 with Improved Photocatalytic Activity Under Visible Irradiation Toward Carbamazepine Degradation. *Materials* 2019, **12**, 3874.
2. P. Šc˘ajev, K. Jarašiūnas, S. Okur, Ü. Özgür, H. Morkoç, Carrier dynamics in bulk GaN. *J. Appl. Phys.* 2012, **111**, 023702.
3. T. Shamirzaev, D. Yakovlev, A. Bakarov, N. Kopteva, D. Kudlacik, A. Gutakovskii, M. Bayer, Recombination and spin dynamics of excitons in thin (Ga,Al)(Sb,As)/AlAs quantum wells with an indirect band gap and type-I band alignment. *Phys. Rev. B* 2020, **102**, 165423.
4. S. Zaheer, S. M. Young, D. Cellucci, J. C. Teo, C. L. Kane, E. J. Mele, A. M. Rappe, Spin Texture on the Fermi Surface of Tensile-strained HgTe. *Phys. Rev. B* 2013, **87**, 045202.
5. W. Zhou, J. Chen, Z. Yang, J. Liu, F. Ouyang, Geometry and electronic structure of monolayer, bilayer, and multilayer Janus WSSe. *Phys. Rev. B* 2019, **99**, 075160.
6. W. Zhou, Z. Yang, A. Li, M. Long, F. Ouyang, Spin and valley splittings in Janus monolayer WSSe on a MnO(111) surface: Large effective Zeeman field and opening of a helical gap. *Phys. Rev. B* 2020, **101**, 045113.
7. J. Qi, X. Li, Q. Niu, J. Feng, Giant and tunable valley degeneracy splitting in $MoTe_2$. *Phys. Rev. B* 2015, **92**, 121403.